LUND UNIVERSITY

FACULTY OF SCIENCE

Department of Physics

Divison of Synchrotron Radiation

Evaluation of Thermal Sensor Calibrations Below 1 K For a Horizontal Dilution Refrigerator in a Cryomagnet

Bachelor's Thesis (15 hp), FYSK04

Supervisor:

Prof. Elizabeth Blackburn

Author:

Samuel Anand

Presented during the January session
Academic year 2025/2026

Acknowledgments

I would like to begin by thanking my supervisor, Professor Elizabeth Blackburn for offering an extremely fascinating and interesting experimental project that opened the world of cryogenics for. She has been very insightful and helpful throughout the project and thanks to her I have learned a lot about research projects. Furthermore I wish to thank her for the opportunity to observe the cryostat in use at a beamline at DESY in an upcoming experiment on supersolids, I am looking forward to being a part of a bigger experiment.

I wish to also thank Dr. Alexander Holmes and Dr. Oleksiy Zadorozhko for being excellent hosts at ESS for the duration of my project; offering invaluable literature recommendations and wisdom on anything from coffee to cryogenics. They, along with the rest of the personnel in the Sample Environment at ESS were very accommodating and helpful during our time there.

Furthermore, I wish to thank my parents for their constant interest in my project, encouragement and unwavering support even across borders. I wish to also thank my friends, local to Lund and those scattered around the globe, from Finland to Australia, who constantly reminded me how fortunate I am to be involved in such an intriguing project.

A special thanks goes to my dear friends Alma Ragnarsson and Nils Nordenskiöld for offering peace and support whilst keeping me grounded during trying times. A huge thank you also goes to Igor Sokolovic with whom I spent countless hours working on our thesis reports together. He offered invaluable insight and assistance on the ins and outs of the bachelor thesis, coupled with much needed encouragement and assurance. I would not have been able to do this without your support. Thanks also to Vanshika Anand for reading through my final draft and offering an external opinion on content and coherence.

Lastly I would like to thank my band, The Rat-Skullz, for offering a cathartic release during our weekly practice sessions through the tunes of Ghost. The countless takes of Dance Macabre and Paranoid gave me the energy to push forth with this project.

Abstract

Accurate thermometry is essential for experiments in cryogenic environments, particularly those using dilution refrigeration to reach milli-Kelvin temperatures. In this thesis, the calibration range of a Cernox CX1050 sensor was extended below its nominal lower limit of 1.4 K. In addition, the response of RuOx sensors at different positions within the dilution refrigerator was examined to assess their stability and accuracy under operational conditions. Controlled temperature sweeps between 250 mK and 700 mK were performed in the mixing chamber of a 17 T horizontal cryomagnet cryostat, with a pre-calibrated RuOx sensor serving as the reference. Resistance values from the Cernox sensor were recorded and fitted using Chebyshev polynomials to generate a reliable calibration curve in this ultra-low regime. Preliminary measurements between 0.7-1.4 K, above the tri-critical point of the 3He–4He mixture, are needed to broaden the effective operating range of the Cernox sensor and validate the findings of this thesis. Together, the investigations on thermometry enable more precise temperature control for future investigations of superconductivity and quantum materials.

List of Abbreviations

CCS - Carbon Ceramic Sensor
CX - Cernox
ESS - European Spallation Source
LS336 - Lake Shore 336 Temperature Controller
LS370 - Lake Shore 370 AC Resistance Bridge and Temperature Controller
MC - Mixing Chamber
OVC - Outer Vacuum Can
PID - Proportional-integral-derivative (controller)
RuOx - Ruthenium Oxide
SC - Sample Cup
VTI - Variable Temperature Insert

Contents

1 Introduction

In scientific applications, conventional refrigeration technologies can be divided into three main categories: absorption refrigeration, adiabatic demagnetization refrigeration and dilution refrigeration [1]. Absorption refrigeration is the principle underlying typical industrial or household refrigerators. Dilution refrigeration exploits the quantum mechanical properties of a ^{3}He–^{4}He mixture to reach milli-Kelvin temperatures. Phenomena such as quantum mechanical effects in superfluids, superconductors, and semiconductors occur only at very low temperatures, close to absolute zero. Dilution refrigerators are therefore a valuable tool for research in the milli-Kelvin range, where these phenomena can be observed. In such low-temperature experiments, it is imperative that cryogenic sample environments are reliably temperature-controlled, as accurate measurement is essential for understanding sample behavior. The user must be able to trust that the dilution refrigerator is actually operating as it should in the necessary regime for their experiment. To ensure this, the thermal sensors within the dilution refrigerator must be meticulously calibrated.

This thesis focuses on the calibration and analysis of thermal sensors in a dilution refrigerator insert, within a 17 T horizontal cryomagnet. The dilution refrigerator employs three types of thermal sensors: Cernox, ruthenium oxide (RuOx), and carbon ceramic sensors (CCS). This project will focus on the Cernox and RuOx sensors as the CCS sensors are used for diagnostic purposes and not under dilution operation. More specifically, this work aims to extend the range of the Cernox thermal sensor and examines the relationship between the temperatures recorded by two RuOx sensors located at different positions in the dilution refrigerator. Both sensors and their response are examined under a dilution operation with the aid of existing data from other thermal sensors and their calibrations. Prior to these operational runs, the cryostat and its respective dilution refrigerator insert had to be serviced and maintained as it had some operational damage from a previous experiment, including a destroyed heater.

2 Theoretical Background

2.1 Dilution Refrigeration

Dilution refrigeration was initially proposed in 1951 by Heinz London [2]. The principle is that, by exploiting the quantum mechanical properties of a mixture of ^{4}He and ^{3}He. At sufficiently low temperatures, a phase shift can be induced, leading to extreme cooling. Dilution was experimentally achieved first in 1964 at Leiden University and the first functional dilution refrigerator was constructed by Henry Hall in 1965 at Manchester University. Through the decades this technology was further developed to accommodate the needs of various users, primarily for the research sector, to reduce cool-down times and increased cooling power. In recent decades the developments in dilution refrigeration driven by the rapidly developing quantum computing industry. The qubits, or quantum bits utilized in transferring information in quantum computing must be kept in stable environments, and as they are sensitive to thermal vibrations, they require very low and stable temperature environments [3]. To maintain such an environment, quantum computers have a dilution refrigerator within their construction. These are generally

rather large, containing many pumping lines.

For dilution refrigeration to occur, helium must first be cooled to the lambda point. For ^{4}He the lambda point is 2.17 K at standard vapor pressure (SVP). Beyond this lambda point, the viscosity and density drop sharply. Beyond 2.17 K, the ^{4}He atoms reach a state of superfluidity [2]. In this state ^{4}He atoms occupy the same, lowest quantum state, meaning they all exhibit the same quantum mechanical properties, and are described by one wavefunction [4]. This kind of fluid is also known as a Bose-Einstein condensate.

The governing principle behind dilution refrigeration arises from the differing spin states of ^{4}He and ^{3}He. The liquid ^{4}He in the mixture used to achieve dilution exhibits superfluid properties below 2.17 K and is in its ground state. Because it has zero nuclear spin, ^{4}He consequently obeys Bose-Einstein statistics. ^{3}He is a lighter isotope with half integer spin ($I_{^3He} = \frac{1}{2}$), meaning it obeys Fermi-Dirac statistics [2]. At temperatures approaching 0 K, whilst ^{4}He exists as a superfluid, ^{3}He can be approximated to a Fermi liquid. The heat capacity and entropy of ^{3}He is approximately a linear function of temperature at this regime. ^{3}He atoms do not have superfluid properties at these temperatures, but can at much lower temperatures than the operating range of dilution refrigerators, at around 2 mK by forming Cooper-pairs in an environment of 1.5 bar relative pressure or more [5]. ^{3}He atoms can however coexist in the superfluid with the ^{4}He atoms and this mixture is still considered a superfluid as a whole. When the temperature of a mixture of ^{4}He and ^{3}He drops below a tricritical point, ^{3}He can no longer coexist and a phase shift occurs.

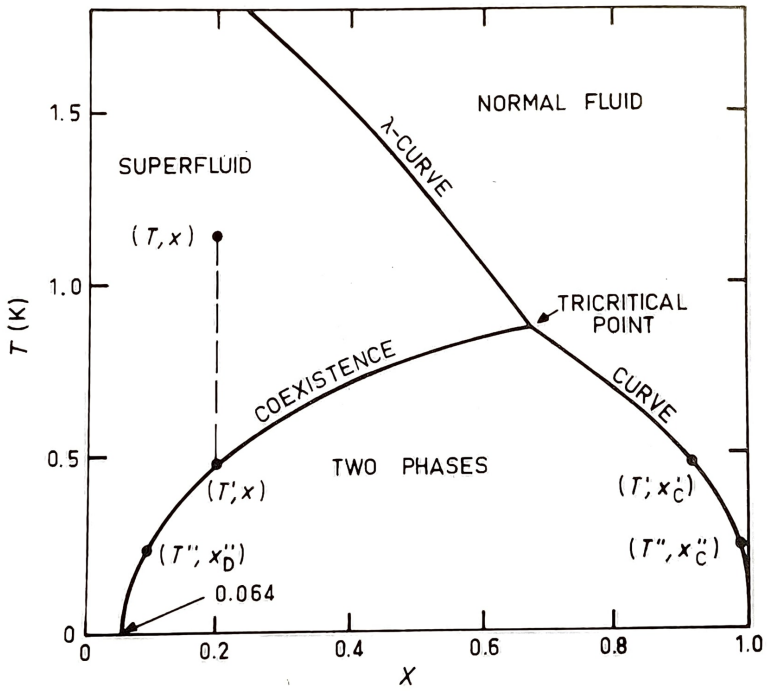

Figure 1: Phase diagram for the ^{3}He-^{4}He mixture extracted from **Fig. 3.1**, from Chapter 3.2 of O. V. Lounasmaa's "Experimental Principles and Methods Below 1 K." It shows the dependency of the properties of the mixture on the concentration of ^{3}He. In the superfluid region, the ^{3}He concentration refers to the percentage of ^{3}He Fermi liquid in the otherwise ^{4}He rich superfluid.

The system is unstable below the coexistence curve seen in 1 and thus must exist above it. This phase shift causes the liquid to sharply split into two separate components, one rich in ^{3}He and another rich in ^{4}He. These are referred to as concentrated and dilute phase respectively, alluding to the concentration of ^{3}He in each phase. The ^{3}He rich (concentrated) phase sits on top of the ^{4}He rich phase as it has lower density. ^{4}He atoms are more strongly bound to the liquid ^{4}He rather than the liquid ^{3}He, the concentration decreases rapidly in the ^{3}He rich phase. As the temperature is decreased below the tricritical point, the concentration of ^{3}He increases in the dilute phase and decreases in the concentrated phase. This can be seen in **Figure 1**, when the temperature decreases, the system can only exist outside the unstable composition, splitting into a superfluid and normal fermi liquid phase. In this figure, at $T' = 0.5$, an initial concentration of x of ^{3}He exists in the superfluid, whilst a concentration of x_c' of ^{3}He exists in the normal, fermi liquid phase. the separation between x, x_c' gives the phase boundary. At T'', the concentration of ^{3}He in the dilute phase decreases and increases in the concentrated phase. A noteworthy feature is that even at 0 K, the mixture must maintain a constant concentration of 6.4% ^{3}He for the operation of a dilution refrigerator [6]. To maintain this concentration, ^{3}He crosses from the concentrated phase to the dilute phase. To cross this phase boundary into the dilute phase, energy corresponding to the enthalpy of change for ^{3}He crossing from the concentrated to dilute phase is required from the surroundings. This directly corresponds to the cooling power of the dilution refrigerator. It is also important to note that determined by the mixture and its parameters, at the point where the phase shift occurs, the mixture will be unstable. This means that controlling the temperature in this specific region will be rather tricky as sudden drops in temperature can occur with slight oscillations.

The cooling as result of dilution is analogous to evaporation, as the ^{3}He concentrated phase acts as the liquid and the ^{3}He dilute phase is the gaseous vapor. As the ^{3}He crosses the phase boundary in dilution refrigeration, it is as a drop of has evaporated, changing from a liquid to a gaseous phase.

2.2 Dilution Refrigerator Layout

The dilution refrigerator used in this project is an insert to the cryomagnet. It is used to cool samples to the milli-Kelvin temperatures that are achievable through dilution. The general structure of a dilution fridge is included in the schematic below.

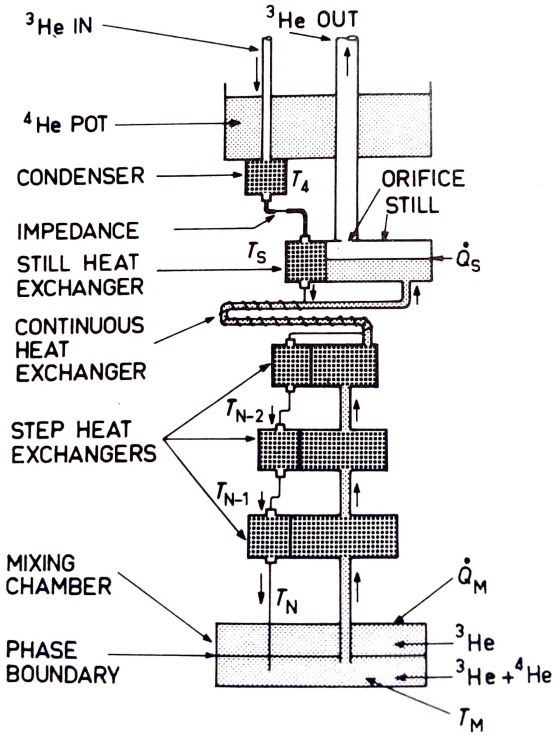

Figure 2: General structure of a dilution refrigerator extracted from **Fig. 3.3**, from Chapter 3.2 of O. V. Lounasmaa's "Experimental Principles and Methods Below 1 K", illustrating the various parts and the flow of the helium circuit.

The first step along the helium circuit in the dilution refrigerator is to liquefy the helium. This is done in the condenser, which is attached to the 1 K pot of the refrigerator. This is a general term for the location at which the condensation occurs as traditionally it is a pot containing ^{4}He, that has a temperature of 1 K. The mixture then passes through a series sintered heat exchangers that are used to cool down the mixture further. This combination of heat exchangers is known together as a step heat exchanger. As the surface area of contact in a sintered heat exchanger is high, so is the thermal conductivity, allowing the liquid to reach such low temperatures. However, as a result, the flow rate has to be constant, allowing for necessary throughput of helium whilst simultaneously avoiding blockages. The sintered heat exchangers come in three levels of coarseness. The finer the sintered powder, the greater the surface area that can be used for heat exchange, but also the flow rate of helium is decreased. For further cooling, continuous heat exchangers are located further along the helium circuit. These are illustrated as a concentric set of pipes, that can be seen in the bottom of **Figure 3b**. Unlike sintered exchangers, continuous heat exchangers simultaneously carry warm and cold liquid through two concentric sets of pipes within a spiral structure. These are counter-flow heat exchangers, with one pipe carrying incoming cold liquid and the other carrying outgoing warmer liquid.

The liquid then reaches the mixing chamber, shown at the top of **Figure 3b**. This is the coldest point of the helium circuit and where the phase separation occurs. The cooling occurs in the mixing chamber of the dilution refrigerator. Here, as the ^{3}He atoms from the concentrated phase move across the boundary to the dilute phase and cooling is produced as a result. Once this separation has occurred, the ^{3}He is driven by an osmotic pressure

gradient [2], back through the heat exchangers and into the still. The still separates the mixture of ^{4}He and ^{3}He into the concentrated and dilute phases. The still then pumps off the ^{3}He, forcing more ^{3}He to flow through the mixing chamber instead. The temperature of the still is a useful indication on whether the phase separation has occurred in the system or not. A sudden drop in the still temperature, followed by a drop in the mixing chamber indicates that the phase separation has occurred.

Figure 3 below display the dilution refrigerator insert used in this project, along with the different components mentioned above.

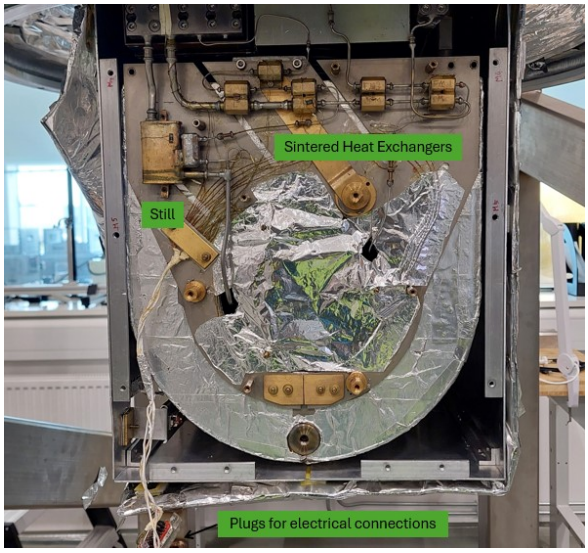

(a) Dilution refrigerator attached to the horizontal cryomagnet.

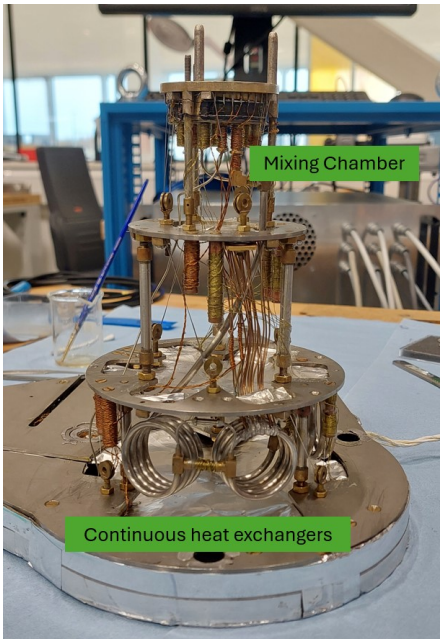

(b) The dilution refrigerator taken outside of the cryomagnet.

Figure 3: The dilution refrigerator insert inside and outside of the cryomagnet with its functional parts labeled.

In this dilution refrigerator the piping for the helium circuit functions as the 1 K pot. One consideration to be made is that since the dilution refrigerator insert sits within the coils of the solenoid and consequently within the magnetic field. ^{4}He has no unpaired electrons, meaning that it is diamagnetic. As a result, it is repelled by magnetic fields. Thus the orientation of the magnetic field must correlate with the design of the dilution refrigerator, and is thus constructed horizontal, unconventional for a dilution refrigerator. Having the still on the outside of the cryomagnet higher than the mixing chamber allows for the exploiting of gravity, both for the flow of liquid helium down to the still and gaseous helium up from the mixing chamber.

2.3 Cryostat Design

2.3.1 Cryostat Schematics

The dilution refrigerator used in this project is part of a larger cryostat. A cryostat is a general term for a vacuum-sealed sample environment that is kept at very low tempera-

tures using cryogens, such as liquid nitrogen or helium. The cryostat was designed and commissioned by Cryogenics Ltd. in 2009. This specific cryostat setup was designed for small-angle X-ray scattering experiments. It was also designed to be portable, to ease transportation between different synchrotron facilities. This particular cryostat is a so called wet cryostat; meaning that it is cooled by cryogenic liquids. Liquid helium has a temperature of 4.2 K. With only the helium tank, the cryostat can thus be cooled down to these temperatures. Samples can be further cooled using the dilution insert.

The whole cryostat is sealed by the outer vacuum canister (OVC), from which air is pumped out under operation. Within this sits three tanks, a 20 l tank for liquid nitrogen, a 40 l tank for liquid helium and a containing the cryomagnet coils. The tank containing helium is referred to as the helium bath. These components are illustrated in technical drawing for the cryostat from the manufacturer included in **Appendix A**.

2.3.2 Cryogenic Seals and Thermal Insulation

To function optimally, the cryostat must be kept in a vacuum to allow for a stable low temperature environment. To keep a stable vacuum, different kinds of seals are used at critical joints. At pipe connection points, greased O-rings are inserted and compressed using clamps. For smaller vacuum seals, such as those within the dilution refrigerator insert, indium is used. Indium is selected as it remains malleable and ductile ever under cryogenic temperatures and does not become brittle, unlike rubber O-rings. Furthermore, the deformed and used seals can be recycled into new seals.

To order to maintain the temperature of the dilution refrigerator constant, thermal shields made of aluminum are placed at different points of the cryostat to protect the system from the external environment. Between these thermal shields multilayer superinsulation is placed to aid with maintaining the cryogenic temperatures required for operation. This superinsulation consists of multiple sheets of aluminized Mylar separated with polyester [7]. The thermal shields work in tandem with the superinsulation to thermally insulate the different sections of the cryostat and maintain the temperatures needed for dilution.

2.3.3 17 T Horizontal Cryomagnet

Beneath the liquid nitrogen and helium tanks are the 17 T cryomagnet's coils. This cryomagnet has been specifically designed for use at neutron and synchrotron facilities to study samples in superconducting states [8]. Cryomagnets used in beamlines typically have a split pair coil design, resembling a Helmholtz coil setup. As the forces between the coils are so large, the maximum strength of the magnetic field generated by this design of magnet is limited. To reach a field of 17 T, this magnet has a solenoid design. A solenoid facilitates strong homogeneity in the magnetic field generated. For superconducting states, and other experiments done under high magnetic fields, low sample temperatures are required. As a result, the magnet comes with two inserts, a variable temperature insert (VTI), and a dilution refrigerator insert to achieve low temperatures. Whilst the VTI allows the sample environment to be in a wider temperature range between 1.5-350 K, the dilution refrigerator insert allows stability for experiments involving lower temperatures, especially below 0.3 K.

2.4 Thermal Sensors

2.4.1 Lake Shore Temperature Control and Resistance Bridge systems

Two main types of thermal sensors are utilized in the dilution refrigerator, Cernox and Ruthenium Oxide (RuO_x) sensors. These thermal sensors measure a resistance value in response to a given temperature, thus assigning a temperature to a given resistance value. The resistance data from these sensors is recorded and processed by a Lake Shore LS370 resistance bridge and a Lake Shore LS336 temperature controller. For this cryostat, the LS336 is used at higher temperature operations and the LS370 at lower temperatures. These temperature controllers operate in slightly different ways. The LS370 employs a Wheatstone bridge to measure the resistance along a resistor. Named after its inventor Charles Wheatstone, the bridge refers to a diamond like configuration of two voltage dividers networks that is commonly used to measure unknown resistances [9]. Wheatstone bridges, or resistance bridges, have a high degree of precision. One advantage of the LS336 is that it has faster control of temperature, however it cannot monitor as many channels, or record resistance as the LS370. For the purposes of this project, the LS370 is used.

2.4.2 Cernox Sensor

Cernox (CX) sensors are made of Zirconium Oxynitride that is formed by sputtering Zirconium in an Oxygen-Nitrogen atmosphere onto a sapphire substrate [10]. A thin Zirconium-Nitride (ZrN) film is the actual sensing element within this sensor. This material is chosen as it has high thermal conductivity at cryogenic temperatures. Cernox thermometers are known for having high sensitivity with fast thermal response and good stability over repeated thermal cycling. Most importantly for applications within a cryomagnet, they exhibit only small calibration shifts under magnetic fields, with a calibration offset ($\Delta T/T$) of 3.2% in fields up to 10 T at temperatures above 2 K [10]. The sensors used are provided by Lake Shore along with a calibration curve. This curve is read by a LS370 or LS336 depending on the operating regime. This allows users to manually alter the calibration curves in response to for example, changing resistances within the circuit. The model of the thermometer that used in this cryostat is the Cernox 1050. The operating regime of this kind of thermal sensor is between 1.4K and 325K. As the nature of the curve is strongly non-linear, the calibration curve between 0-10 K is plotted in **Figure 4**. For the full calibration curve, refer to **Figure 15** in **Appendix B.**

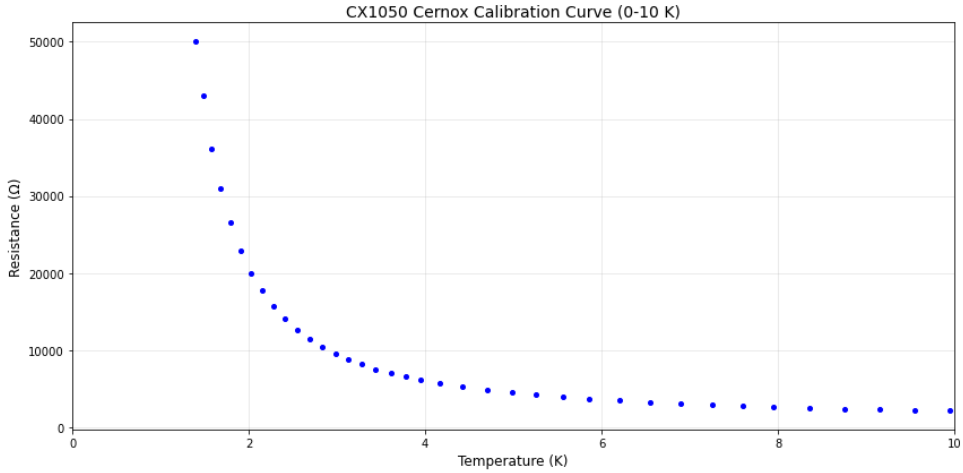

Figure 4: The calibration curve for calibration points between 0 and 10K.

The lowest calibrated temperature value is at 1.4K, corresponding to a resistance of 50104.468 Ω. The full values of the calibration points are included in **Appendix B**.

2.4.3 Ruthenium Oxide Sensor

The RuOx sensors on the other hand are trickier to calibrate; and some of the sensors installed in the cryostat were bought pre-calibrated. Their operating temperatures are much lower: 10mK-2K. Therefore, these are used closest to the mixing chamber, where the dilution refrigeration occurs and such temperatures are reached. These sensors also exhibit low magnetoresistance, which is advantageous for our applications, meaning under high magnetic fields, the calibration does not shift relatively as much under high magnetic fields [11].

2.5 Sensor Calibration

Both RuOx and Cernox sensors work by associating a measured resistance to a temperature value. These temperature values and corresponding resistances are measured experimentally by using another, calibrated sensor, in the same region as the sensor that is to be calibrated. Resistance is measured by the target sensor for calibration; by knowing the temperature from a another calibrated sensor, the two can be matched, assigning a temperature to this resistance. This can then be put onto a calibration sheet. Lake Shore has its own curve handling software which is used for interpolating the values obtained from these temperature control experiments, fitting the calibration curves.

2.5.1 Numerical Fitting Using Chebyshev Polynomials

Whilst Lake Shore does not explicitly mention the fitting method its software uses, common operating procedure in cryogenics is to use Chebyshev polynomials. For these fitting purposes, Chebyshev polynomials of the first kind are used. These are a collection of orthogonal polynomials that are solutions to the Chebyshev differential equations [12].

Chebyshev polynomials of the first kind are defined on the interval [-1,1] by the following recurring relation.

$$T_{n+1}(x) = 2xT_n(x) - T_{n-1}(x). \tag{2.1}$$

The first few Chebyshev polynomials are thus given as follows.

$$\begin{aligned} T_0(x) &= 1 && \text{(degree 0)} \\ T_1(x) &= x && \text{(degree 1)} \\ T_2(x) &= 2x^2 - 1 && \text{(degree 2)} \\ T_3(x) &= 4x^3 - 3x && \text{(degree 3)} \end{aligned}$$

Where n denotes the order of the polynomial. To numerically fit calibration data that spans [T_{min}, T_{max}] instead of the defined interval of [1,1], this temperature is mapped to a standard interval using the following linear transformation:

$$x = 2(T - T_{min})/(T_{max} - T_{min}) - 1. \tag{2.2}$$

The explicit trigonometric definition of the Chebyshev polynomial is given below in **Equation 2.3**

$$T_n(x) = \cos(n \arccos x) \tag{2.3}$$

where n is the order of the polynomial.

Because of the highly non-linear nature of such calibration curves, common operating procedure in cryogenics is to fit the resistance with respect to $\log_{10} R$ for more accurate fitting and interpolation. To approximate $\log_{10} R$ as a function of T, the Chebyshev series, a sum of Chebyshev polynomials is used. The series is given in **Equation 2.4**.

$$\log_{10}(R) \approx \sum_{i=0}^{n} a_i\, T_i(x) = a_0T_0(x) + a_1T_1(x) + a_2T_2(x) + \cdots + a_nT_n(x) \tag{2.4}$$

where a_i are the Chebyshev coefficients and n is the polynomial degree. By substituting with the first few Chebyshev polynomials into the series, it is expanded as follows

$$\log_{10}(R(T)) \approx a_0 \cdot 1 + a_1 \cdot x + a_2 \cdot (2x^2 - 1) + a_3 \cdot (4x^3 - 3x) + a_4 \cdot (8x^4 - 8x^2 + 1) + \ldots \tag{2.5}$$

When fitting calibration curves, it is a good idea to do so in segments, as Chebyshev polynomials are rather sensitive and can fluctuate a lot. This means that different segments of the curve will be governed by different equations. The resistance values measured over the operational range of a Cernox sensor, for instance, can span over 3 orders of magnitude. Aside from interpolation, Chebyshev polynomials could be used to extrapolate the calibration curve of a sensor. One should be skeptical when using Chebyshev polynomials for extrapolation purposes as high degree polynomials exhibit rather unpredictable behavior outside the fitted interval. Furthermore, the physical relationship between temperature and resistance may change its form. Thus, the more reliable method for extending the calibration of the sensor is to conduct temperature control measurements at the desired temperature, to get a value for the resistance.

2.6 PID Temperature Control

To heat a resistor and achieve a desired temperature within the cryostat, proportional-integral-derivative, or PID, controllers are used to maintain a stable temperature. This PID modulates the input power on the resistor to reach the desired temperature. Each term of a PID controller, so the proportional, integral and derivative terms alter the input signal in their own way. The proportional term is used when one wishes the controller action to be proportional to the size of the process error signal [13]. The integral term is used to correct for a steady offset and similar long term deviations from the setpoint, by integrating the error signal. The derivative term is more delicate as this term considers and anticipates error changes in the future. The sum of these terms give the control output. For the cryostat, the PID controller's parameters can be altered in the Lake Shore 370 resistance bridge. The PID control equation for this specific model is extracted from the device manual and given below [14]

$$\text{Heater Output} = P\left[e + I\int(e)dt + D\frac{de}{dt}\right] \tag{2.6}$$

where P is the proportional term, e is the error, defined as setpoint temperature minus feedback reading. Adjusting the different parameters of the PID controller can improve the stability of the temperature. This is especially important for experiments that use the dilution refrigerator. These experiments generally require low and stable temperatures, therefore an accurate and reliable PID control is imperative.

3 Experimental Method

3.1 Preface and Protective Measures

The cryostat used for this experiment was stationed in the Sample Environment at the European Spallation Source (ESS), on the outskirts of Lund. The cryogenics required for keeping the system cold, namely the liquid nitrogen for pre cooling and the helium (^{4}He) for operation was supplied by ESS and returned through their helium recovery system. The ^{3}He-^{4}He mixture needed to achieve dilution is stored within the cryostat's gas handling system that and runs on a separate circuit as the cryogenics used for cooling. Furthermore, indium used for seals were supplied by ESS. The indium that was removed from the seals was recycled back to them.

When working with cryogenics, the temperatures of the liquids involved are very low and it is important to use cryogenic gloves when working with cold surfaces and liquids. Liquid nitrogen sits at a temperature of 77K. Whilst splashes and quick contact to the skin are not very harmful, prolonged content can lead to frostbite. Liquid helium on the other hand is at 4.2K. Here even instantaneous contact can cause severe burns and damage to the skin.

3.2 Dismantling

The cryostat was hoisted onto a a platform using a crane, easing access to the dilution refrigeration insert. The insert was damaged during a previous experimental run at DESY

in Hamburg and had to be repaired now. To begin the necessary maintenance work on the insert and its respective sample cups, the insert was removed following a meticulous process. The superinsulation is removed using gloves to not damage the insulation. Once all the shields are removed, support manifolds are placed onto the dilution refrigerator to support the delicate piping and heat exchangers during the removal and prevent their bending. Indium seals that were on the connectors are removed using isopropyl alcohol and recycled. Now the dilution refrigerator insert is removed from the cryomagnet and is ready to be worked on.

3.3 Maintenance Work on Dilution Refrigerator

Before re-installation of the dilution insert for testing purposes, maintenance work, the insert is fixed. A resistor on the mixing chamber had detached out of place and had to be glued onto the body of the dilution refrigerator. The mixing chamber is illustrated in **Figure 5** below.

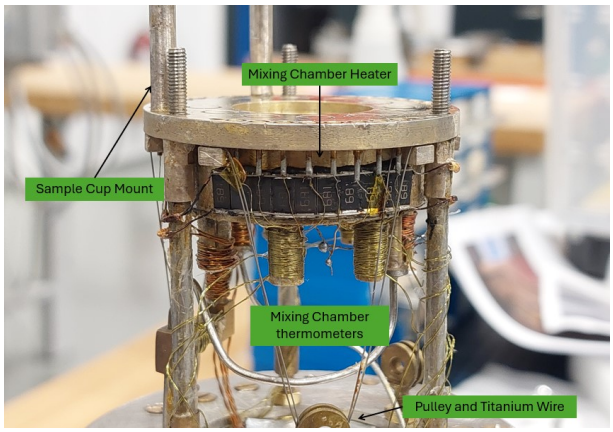

Figure 5: The heaters surrounding the mixing chamber.

The different levels of the dilution refrigerator are suspended using a wire and pulley system akin to those found on satellites. This system is visible in the bottom of **Figure 5**. By altering the tension on the wires made of titanium, the tension on the wires and thus the orientation of the levels can be altered. One of these wires had snapped and had to thus be replaced.

3.4 Maintenance Work on Sample Cup

A sample cup which is mounted onto the dilution refrigerator had to be serviced. The sample cups are made of silver with a small percentage of palladium. The sample cup is illustrated in **Figure 6.**

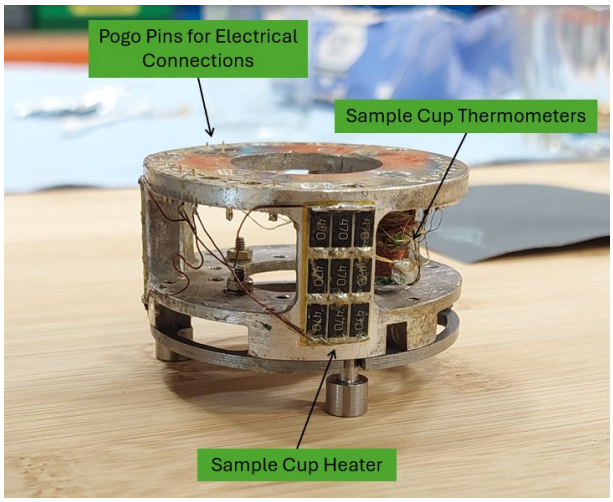

Figure 6: Sample cup used for mounting samples onto the dilution refrigerator.

During a previous operation of the cryostat, some of the surface mounted (SMD) resistors used as heaters for temperature control had burnt and needed replacing. The sample cups use SMD resistors to improve thermal conduction over the surface of the sample cup. A resistance of about 30 Ω is required from these heaters. To achieve this an array of resistors with a total resistance of 48 Ω is used instead of a single resistor to further improve the heat dissipation over the surface of the sample cup and the resistors. On the sample cups specific to this dilution refrigerator setup, the resistors are mounted in two arrays in series, each consisting of 3 resistors in series and 3 in parallel, as illustrated in **Figure 6**. This gives a total resistance of 24 Ω. To ensure the resistors do not make electrical contact with the surface of the sample cup, the resistors are attached to a piece of Kapton tape, which is a thin, insulating polyimide film. Kapton remains stable through a wide array of temperatures. This tape is fastened to the resistors and then glued onto the sample cup using a special glue that can be thinned with acetone. They were removed from the surface of the sample cup. An array of resistors from another sample cup was recycled, and soldered onto the sample cup that needed maintenance. The wires have an insulating coating that was removed using fine grit sandpaper prior to soldering.

The sample cup also has a RuOx and a CX thermal sensor. These are connected to spring loaded push-pin style connectors, or pogo pins from which the readings can be extracted. Over time, these pogo pins get bent and worn out. Some of the pins on the sample cups were rather damaged and had to be replaced. The solder connecting the wires to the pogo pins was removed, and the pin taken out of its Teflon insert. A new pin was placed and the wire soldered back by tinning the wire and the pin, and then soldering a joint such that the wire is inserted within the pogo pin. Care was taken to ensure the correct wire was soldered to the correct pin, crucial for reading the data.

3.5 Testing Electrical Connections

Once the cryomagnet is cooled down for operation, access to the internal components and the dilution refrigerator insert is incredibly limited as the apparatus will be under a vacuum. Therefore, before mounting the insert onto the cryomagnet, the various electrical connections from the insert needed to be verified. The insert has 3 different plugs that

will be connected to the cryomagnet, for measuring externally, without having to open up the cryomagnet. Using a multimeter, the resistance over a component was measured. These components included heaters placed around the still, mixing chamber and heat exchangers, along with various places along the manifold. The measured resistance was compared to the expected resistances of these sensors. These connections were also tested for electrical shorts to ground. This is done by placing one probe on the pins and another on the aluminum casing of the cryostat. Once satisfied that the resistance values along the connections is as expected and no electrical shorts are present, the insert is plugged into the cryostat. Now the electrical connections, and thus the different components are be measured externally using a control rack and a Lake Shore signal processor. This signal processor gives both the resistance value, and the corresponding temperature of the thermal sensor. This temperature is calculated using an uploaded calibration curve. This measurement is taken to ensure no electrical shorts occur within the wiring of the cryostat itself.

3.6 Setup for Temperature Control Measurements

After the maintenance work has been conducted, the cryostat is sealed and hoisted onto the trolley with a crane.

For the cryostat to achieve dilution, a gas handling system is attached to the cryostat using pipes. This bespoke gas handling system controls the flow of helium within the dilution insert. It also contains the ^{3}He-^{4}He mixture that is necessary for achieving dilution. This system is also used to maintain the pressure within the system, allowing the user to monitor for blockages and maintaining constant flow within the system whole system. The gas handling system is shown in **Figure 7a**. **Figure 7b** shows the different valves that can be controlled using the onboard computer. Aside the gas handling system

(a) Gas handling system of the cryostat.

(b) Screen of the gas handling system.

Figure 7: The gas handling system of the cryostat and the screen displaying the circuit.

a control rack is also attached using the various electrical connections at the top of the

cryostat. The control rack contains the Lake Shore™LS336 and LS370 used for monitoring and controling the temperature, a heater to prevent a known superleak[1] in the system and a computer. Using this computer, the measured values for the temperature resistance across all the active channels connected to the LS370 are logged. These values are also plotted and displayed on a monitor allowing the observation of the temperature. The needle valve, which regulates the flow of ^{4}He for cooling the cryostat can be controlled from the computer.

3.7 Pre-cooling and Filling of Helium and Nitrogen Tanks

Before precooling, using a turbo pump, the air within the cryostat is pumped out to create a vacuum. Once pumped a leak test is done to ensure the seals within the piping are airtight. To do this a leak detector is connected to the pump, and helium from a pressurized helium tank is sprayed with a helium spray gun around the different seals.

As the cryomagnet has been sitting in room temperature throughout the previous steps of the maintenance process, if the system was filled with helium, most of it would evaporate. To stop this from happening and wasting the expensive and precious helium, the system needs to be initially cooled down in a process known as pre-cooling. Through this process, the nitrogen and helium baths of the cryomagnet are filled with liquid nitrogen. For this, a gas handling system is attached to the cryomagnet to control the various valves in the system. The liquid nitrogen is pumped in and left overnight to cool down the system to about 77 K. The nitrogen is pumped then pumped out into a container called a trap, separate from the system.

Once the system is at a sufficiently low enough temperature, helium can be pumped into the system. Initially only helium gas is pumped through the cryomagnet to further cool the system in preparation for the pumping of liquid helium. A dewar flask containing helium at atmospheric pressure was connected to the cryomagnet using a siphon. The pressure within the dewar is increased by adding heat with a heater to initiate the siphoning of the helium from the dewar into the cryostat. Initially, the gas is pumped through the bottom of the entire structure, allowing helium gas to pass underneath the coils of the cryomagnet. This ensures the entire system is cooled with the helium and not just the top, as the helium gas rises through the system. Next the liquid helium is pumped into the helium bath, up to 230 mm, the maximum level of the 40 l helium bath.

3.8 Conducting Temperature Control Measurements

Measurements of temperature readings were collected for calibration purposes. The readings are processed by the Lake Shore LS370, which collects both the measured resistances and calculates the corresponding temperatures using the calibration curves input by the user. The LS370 only measures the resistance but assigns the temperature to the measured resistance using the points from the calibration curve that is input into the LS370. For conducting our measurements, the RuOx heater on the mixing chamber is used for temperature control through the physical LS370 unit. A setpoint temperature is input onto the device and a heating power selected. The PID values were set at 0.5s for the

[1] A superleak is a leakage through which regular fluid cannot flow through as the viscosity of a regular fluid prevents it, however as a superfluid, the liquid exhibits zero viscosity [2].

proportional term, 2s for the integral term and 2s for the derivative term. These were varied as needed to provide stable temperature control from the control rack. Using the computer on the control rack, the data recorded was observed graphically and saved as a txt file. Initially, 9 microwatts of heat was supplied through the resistor to raise the temperatures in steps of 50mK. The PID settings were kept at 5,2,1 for the proportionality, integral and derivative settings respectively. The temperature was controlled in steps of 50mK from 250mK to 900mK.

Once the measurements were collected, the resultant temperature a RuOx sensor, connected to channel 7 on the LS370 and a CX sensor connected to channel 6 on the LS370 on the sample cup were observed for stable regions. Using the data points for the resistance measured on the CX and the corresponding temperature on the RuOx sensor, the two were matched, allowing for the extension of the calibration curve of the CX beyond its operational range assigned by the manufacturer. This allows for further validation of the temperature as now two sensors are measuring at this region.

4 Results

4.1 Temperature Control

Through the data measurement runs, data from all the connected sensors in the LS370 are recorded. For this investigation, three specific sensors are of interest, the RuOx sensors on the mixing chamber and the Cernox sensor on the sample cup. The first two provide reliable readings for low temperatures; the resistance measured on the Cernox will be recorded. **Figure 8** below is an example of one of the temperature control measurements conducted at 300 mK, illustrating behavior of the temperatures at the sample cup and mixing chamber. The sample cup temperature is given by the blue curve and the red illustrates the mixing chamber temperature. The plots of all measurement runs used for this analysis and investigation are enclosed in **Appendix D**.

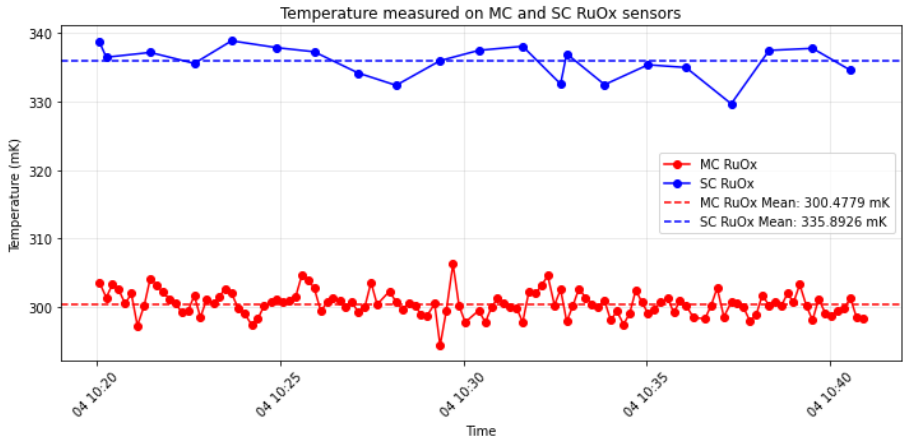

Figure 8: Temperature recorded by a RuOx sensor on the mixing chamber and sample cup whilst controlling at 300 mK. This data was on 4.12.2025 between 10:20am and 10:40am.

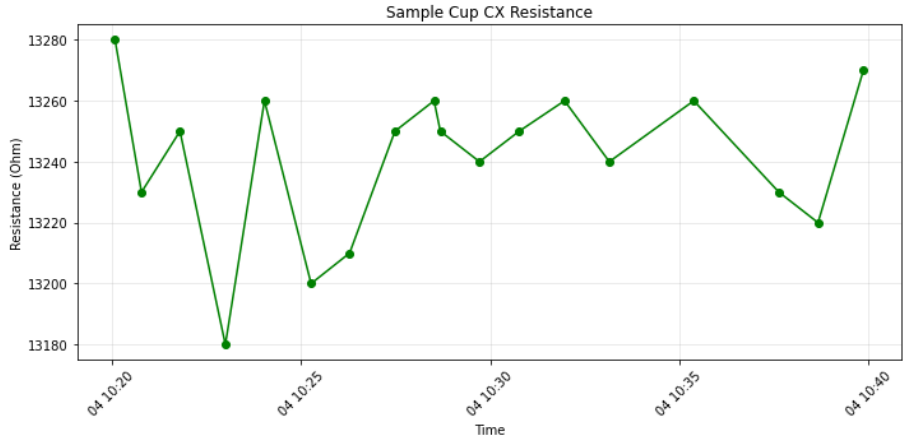

Figure 9: Resistance recorded by Cernox sensor on the sample cup whilst controlling at 300 mK. This data was extracted on 4.12.2025 between 10:20am and 10:40am.

As the temperature was controlled using the mixing chamber heater, the LS370 cycles through the corresponding channel more frequently, producing more data points. This is illustrated in **Figure 8** with the blue curve, the sample cup RuOx sensor, having fewer points than the mixing chamber sensor. This is also seen in **Figure 9**, which also has a less frequent sample rate. The red curve for the MC RuOx sensor exhibits a strong linear trend, illustrating reliable temperature control. The blue curve tends to oscillate a bit more, but still displays a strong linear trend. This observation is consistent throughout the temperature control runs at different temperatures. This is further confirmed by observing the data and errors in **Table 1** below, where the average value was taken over the dataset.

Table 1: The controlled temperature, temperature values measured on the RuOx sensors in the mixing chamber and on the sample cup and the resistance values measured along the sample cup Cernox.

Control T (mK)	**MC RuOx T (mK)**	**SC RuOx T (mK)**	**SC Cernox R (Ω)**
250	253.36 ± 2.26	275.85 ± 3.67	12771.04 ± 46.86
300	300.48 ± 1.81	335.89 ± 2.33	13241.45 ± 23.68
350	351.47 ± 1.93	389.21 ± 1.22	13386.46 ± 29.38
400	399.64 ± 5.13	435.143 ± 3.22	13286.09 ± 13.05
450	449.43 ± 6.64	491.99 ± 6.10	13252.11 ± 39.32
500	497.85 ± 16.36	531.48 ± 0.76	13272.0 ± 17.7
550	544.41 ± 11.10	569.41 ± 12.16	13676.64 ± 30.95
600	575.70 ± 8.43	603 ± 8.80	13852.48 ± 21.45
700	688.04 ± 16.35	722.23 ± 4.76	13105.00 ± 118.26

The error value on the mixing chamber RuOx offers a notion of how reliable the temperature control is. For instance, temperatures between 500-700 mK display the largest error values, suggesting temperature control was difficult in this region The duration of these measurements were taken over 4-5 minutes of temperature control, however for measurements for 300 mK remained stable for 20 minutes, and thus the data was averaged over this period of time. A longer measurement time would mitigate random errors, however

as limited time could be spent in the lab, 5 minutes of stable control was established for the other data sets.

The measurements were intended to be conducted in steps of 50 mK between 0-1 K as this is below the effective range of the Cernox sensor, the calibration of which was to be extended whilst being within the effective range of the RuOx sensors, whose behavior and interplay was examined. Reliable data points could only be collected between 250-700 mK. As the dilution refrigerator was not operating most efficiently, the lowest temperature achieved during this experimental run was 200 mK. A region of instability was observed whilst conducting measurements around 650 mK. This was reflected by large fluctuations in the data. This is further backed by an increase in the error values for all the measured sensor channels in **Table 1**. Through many experimental runs, accurate control of the temperature at 650 mK was not achieved, with further difficulty at temperatures higher than this.

Whilst conducting the temperature control measurements at temperatures below 1 K, there was initial difficulty in maintaining the temperature upon heating the mixing chamber. This was indicative of some issue. Upon raising the temperature, occasionally it would drop down drastically with the mixing chamber at around 600 mK. This instability suggests that phase separation, so dilution is occurring, but not at the expected range. A possibility is that as helium gas evaporates, it releases some blockage of liquid helium within the system, allowing the mixture to undergo dilution.

Furthermore, the phase separation does not seem to be occurring at the mixing chamber. This is further backed by the fact that the temperature of the still was around 1.3 K for most of the temperature measurements. This is higher than the expected temperature, the tricritical point for the mixture, suggesting that only ^{4}He is going through the still. Hereby, the phase separation is thus occurring elsewhere in the circuit of the dilution refrigerator, as is the pumping effect of the still. Consequently, the pumping is not at its most efficient, leading to further instability in the mixture. The initial difficulties with achieving dilution could be attributed to the still being at a higher temperature, as the phase boundaries have shifted to another part of the circuit. The lowest temperature achieved during the whole experimental run.

A heat leak in the form of a touch, where thermal contact is made between parts within the dilution refrigerator was originally theorized as the reason for this difficulty in achieving dilution as it could lead to a leakage of heat from the system. However, whilst sealing the dilution refrigerator and the cryostat up for operation, no such touch was visibly observed. A touch would also lead to much higher temperatures than what was observed. This conclusively suggests that the circuit not operating as it should have is the likely reason why dilution was hard to achieve, and why overall the dilution refrigerator was operating at a higher temperature than expected.

The temperature control measurements were conducted over a period of several days. During this time, due to instabilities in the system such as unwanted pressure buildup in the circuits within the helium return system and the system not achieving dilution at the intended locations, the amount of ^{3}He-^{4}He mixture was altered. This impacts the temperatures and could have shifted the instability region.

The PID settings play an important role in achieving stability in temperature control. Therefore altering the PID settings can improve the control of the temperature in stable regions. The optimal PID settings varied through different temperature ranges. Having

a strong understanding of how the temperature control behaves in response to different PID inputs, can help stabilize the temperature control, minimizing the resultant errors in the data. The ideal settings for each component is not defined but rather found out experimentally, by observing the response in the temperature oscillations to different inputs. This is a rather iterative process and thus very time consuming. Through previous experimental runs, a PID setting of 0.5,2,1 was found to be optimal for measurements under 250 mK. No information was however given for temperatures above this. I discovered that a PID setting of 0.3,2,2 was the optimal setting for measurements between 350-600 mK. Different PID settings were tested for temperatures of 650 mK and above, however as this determined to be a region of instability for this system, controlling the temperature was difficult regardless of the PID setting. Given more time, the process of heating and controlling the temperature using the right PID inputs could be streamlined.

A separation is observed between the average temperatures of the two thermal sensors. This is expected as the two thermal sensors are located at different parts of the circuit. The behavior of this separation is important to understand as whilst the temperature is controlled on the mixing chamber, the sample cup temperature is vital to understand as the samples are housed there. Understanding this relationship will give a better idea as to what temperature the sample is actually experiencing. The variation in this separation for the same temperature control run conducted at 300 mK is given in the plot below.

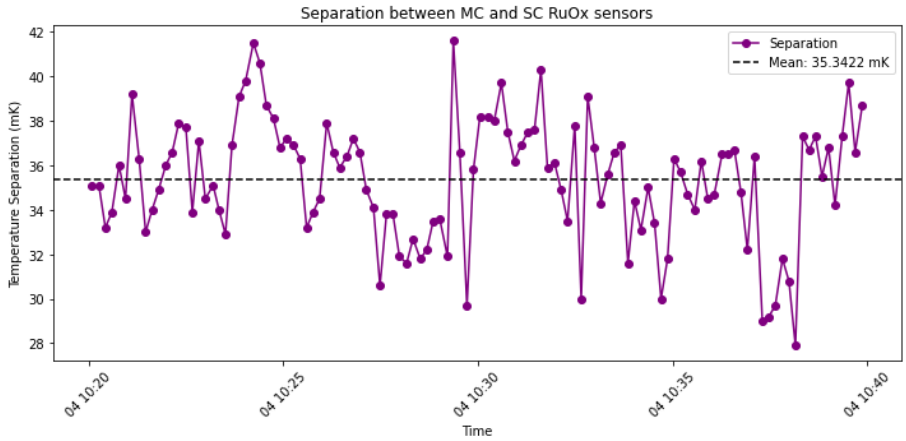

Figure 10: Temperature separation between the MC and SC RuOx sensors at 300 mK control temperature.

Over a temperature control run, 10 illustrates a linear trend in the separation between the two sensors, from which a mean value can be extracted. However, as illustrated in the following plot, such a clear distinction in the trend of the separation between sensors cannot be made over all of the temperatures. It is further observed that the separation also tends to vary a bit. To study the trend over the whole dataset, the values for the separation of the two RuOx sensors at each control temperature, so $T_{SC} - T_{MC}$, is plotted in **Figure 11**.

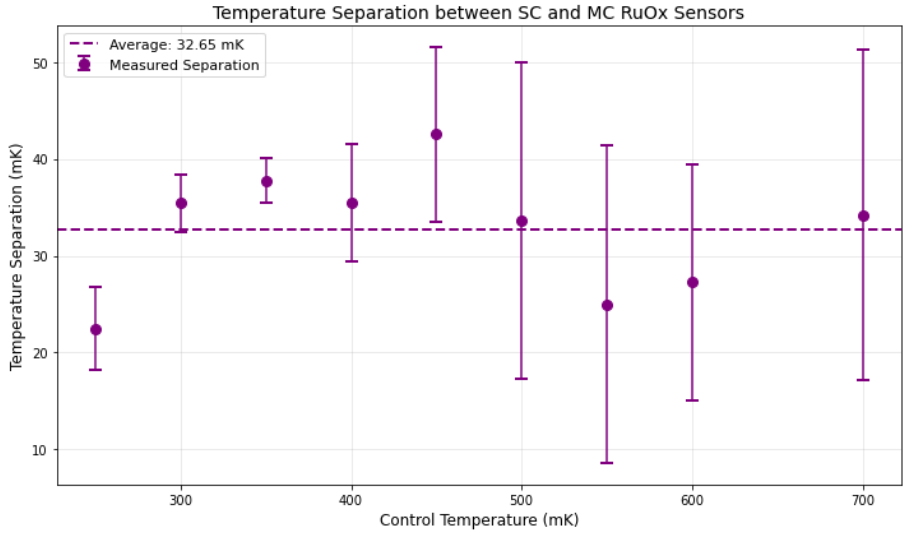

Figure 11: Separation between SC and MC temperatures

The average separation of the values is calculated to be $32.65 \pm 6.09\,\text{mK}$. This means the sample cup is warmer than the mixing chamber, which makes sense as the mixing chamber is traditionally the coldest part of the circuit, as the phase boundary lies within. Upon plotting, a clear trend in this separation is not visible from the figure. This average values assumes a linear trend, that the temperature is only offset. However a line of best fit could show an increasing trend. What is observed is that the error increases with higher temperatures. This can be explained by the aforementioned areas of instability and difficulty in temperature control around and above 650 mK. To better understand the behavior of this trend and whether the separation does increase with increasing temperature, more data from temperature control experiments above 700 mK is needed.

4.2 Calibration Curve Extrapolation and Extension

One of the primary objectives of this project is to evaluate whether the calibration of the Cernox sensor can be extended such that the Cernox could read temperatures below 1 K. get an idea of the kind of resistance values expected to be measured in this interval, the existing CX1050 curve is extrapolated. Using a numerical Chebyshev fitting, the original calibration curve is extrapolated using data points from 1.4-4.2 K. The resultant function is optimized as a 7th degree polynomial, given in **Equation 4.7**.

$$\begin{aligned}\log_{10}(R) = {} & 9.20727 - 8.36184\,T + 6.92544\,T^2 \\ & - 3.5228\,T^3 + 1.11491\,T^4 - 0.214572\,T^5 \\ & + 0.0230168\,T^6 - 0.00105627\,T^7\end{aligned} \tag{4.7}$$

The resultant curve is plotted as R vs T in **Figure 12**. The corresponding resistance values 250-700 mK are included in the table below.

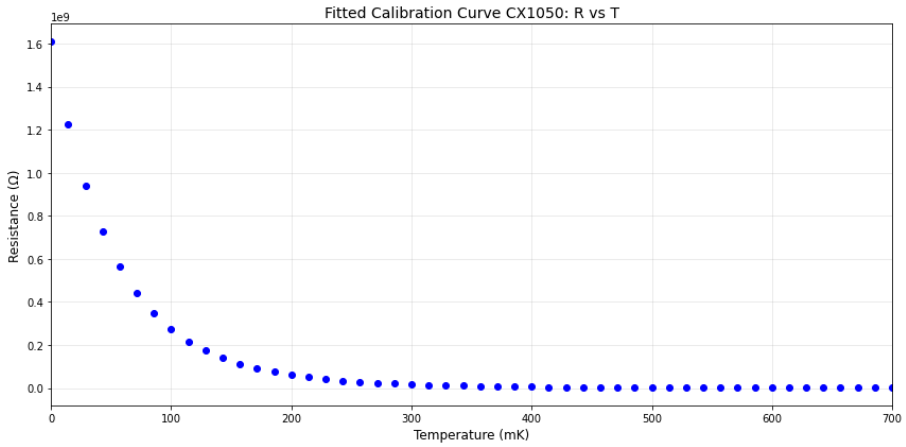

Figure 12: The extrapolated calibration curve of the CX1050 Cernox sensor plotted between 0-700 mK.

Table 2: Control temperatures and their corresponding resistances from the extrapolated calibration curve for the CX1050 Cernox.

T **(mK)**	R **(Ω)**
250.00	31 532 425.56
300.00	17 195 622.77
350.00	9 853 661.23
400.00	5 909 928.48
450.00	3 696 361.60
500.00	2 402 635.48
550.00	1 617 860.04
600.00	1 125 255.44
650.00	806 175.11
700.00	593 437.37

When comparing the experimentally measured values with the values given by the Chebyshev fit of the calibration curve, a clear difference of many orders is noticed. This Chebyshev fitted curve should only be used to give a notion of the trend. The calibration curves of these thermal sensors are fit in segments, and as these temperatures are below the tricritical point.

To visualize the trend of the measured resistance values along the Cernox sensor, the temperature measured by sample cup RuOx sensor is plotted against the resistance measured from the Cernox in **Figure 13** below.

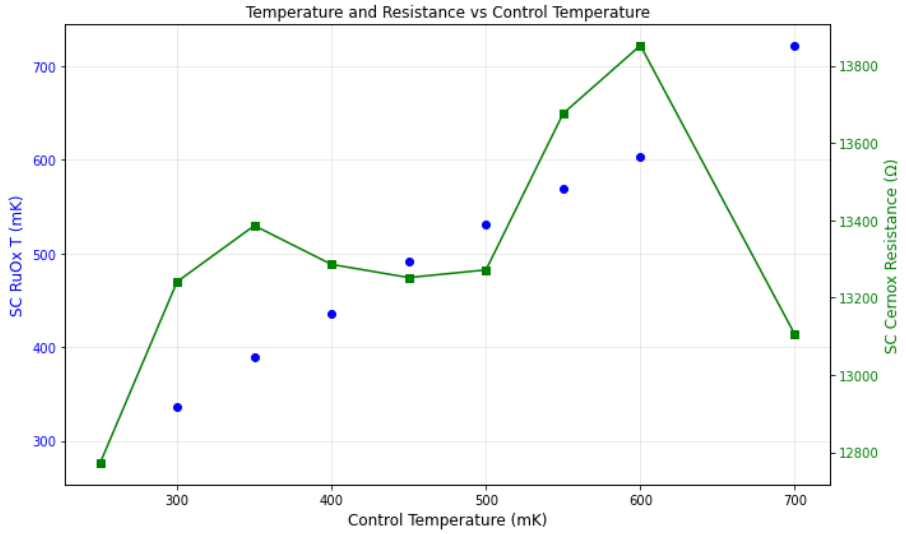

Figure 13: Temperature recorded on the sample cup RuOx and the resistance measured on the Cernox plotted against the temperature.

To further visualize the full trend of the calibration curve with the acquired experimental data, the updated calibration curve between 0 and 3 K is illustrated in **Figure 14** below.

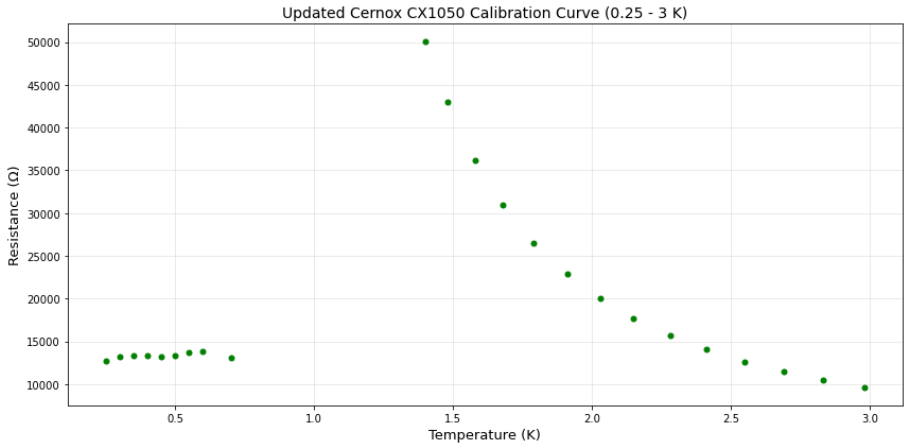

Figure 14: Calibration curve for the Cernox CX1050 sensor with acquired experimental resistance data.

Figure 14 illustrates that the behavior of the new experimentally acquired values is rather different than the original calibration curve, exhibiting a quadratic relation rather than an exponential one that was expected from the extrapolation. To verify the nature of this trend, more data points would be needed as the trend is not very conclusive from this data. Furthermore, as the trend does not exhibit strong exponential behavior, Chebyshev polynomials cannot be used to fit this newly obtained calibration curve segment.

From examining the calibration sheet for the CX1050 Cernox sensor used, the lowest calibrated temperature on the curve was 1.4 K. The resistance corresponding to this temperature is 50104 Ω. By observing the data obtained through the temperature control measurements, this is well above the measured resistance at 700 mK, 13105 Ω. This measured resistance would correspond to a value between 2.41-2.55 K, meaning the same

resistance would be measured at two different temperatures. This suggests that the resistance curve changes direction at some point between 0.7-1.4 K as until this point, the resistance increases with decreasing temperature, according to the calibration points. To further validate the idea that the curve switches direction, more temperature control measurements are needed to study the relationship between the resistance measured and the control temperature between the whole range up to 1.4 K. This would also help in the fitting of this second curve. An interesting note is that the behavior of this curve is similar to that expected from the temperature resolution curve provided in the documentation for the Cernox sensor by Lake Shore [10], showing an increase in resistance, followed by a drop, and another, smaller increase.

5 Conclusion and Outlook

This bachelor project combined essential maintenance work with scientific calibration to strengthen the operation of a dilution refrigerator within a 17 T horizontal cryomagnet. The core aim of the was to improve the calibration of a Cernox thermal sensor on a sample cup connected to the dilution refrigerator to evaluate the possibility of extending it past the manufacturer's recommended operational range and to study the behavior and relationship under temperature changes of two RuOx sensors located on the mixing chamber and the sample cup. Considerable time was devoted to servicing the cryostat and its insert, including dismantling, repairing damaged components, soldering heaters and electrical connections and replacing pogo pins on the sample cup. These tasks were critical to restoring the system to reliable working order and provided the foundation for the calibration experiments.

Temperature control was most stable over 250-700 mK so values for resistance on the sample cup Cernox, and the temperature measured on both the mixing chamber and sample cup RuOx sensors were recorded. Using the calibration, temperature values were assigned to the Cernox thermometer. From observing these values, it was concluded that the initial calibration curve could not be extended using Chebyshev polynomials to facilitate the resistance values, as the behavior was not as expected. Instead it is suggested for temperatures below the lowest operating range (1.4 K), a new calibration curve is fitted. To validate this, resistance values at temperatures between 0.7-1.4 K is needed to reliably fit a calibration curve.

Another objective of this project was to investigate the relationship between the sample cup and mixing chamber RuOx sensors, namely the difference of their readings as a function of mixing chamber temperature. This is important when controlling the mixing chamber temperature in experiments as the sample cup, and subsequently the sample, will be at a different temperature. Knowing this offset will help accurately control the temperature in the sample cup and understand the behavior of the sample. It was discovered that on average the sample cup was 32.65 ± 6.09 mK warmer than the mixing chamber. Upon plotting a clear trend was not observed, it is however possible that this separation increases with increased temperature. To validate this outcome, once more data points for temperatures above 700 mK are needed to conclusively determine a trend.

Together, the maintenance, setup, and calibration work carried out in this thesis have ensured that the cryostat is fully operational. These results provide a stronger basis for precise temperature control in the milli-Kelvin regime for this cryostat. The next step

would be to update the calibration curve of the Cernox sensor on the mixing cup and conduct measurements to evaluate and validate the accuracy of this Cernox. The cryostat is due to be used in an experiment at DESY, Hamburg in January 2026 concerning the experimental study of supersolids. This would be a good opportunity to test the new findings of this investigation calibration curve, as this experiment requires an environment of 200 mK, meaning the dilution insert will be used. Whilst the Cernox needs further data to be reliably calibrated further, the findings from the temperature separation investigation on the sample cup and mixing chamber RuOx sensors will prove useful in the context of this upcoming experiment to provide a stable and controlled temperature for the sample to be studied.

References

[1] H. Zu, W. Dai, and A. T. A. M. de Waele. "Development of dilution refrigerators: A review". In: *Cryogenics* 121 (2022), p. 103390. DOI: 10.1016/j.cryogenics.2021.103390.

[2] O. V. Lounasmaa. *Experimental Principles and Methods below 1 K*. Academic Press, 1974.

[3] S. Krinner et al. "Engineering cryogenic setups for 100-qubit scale superconducting circuit systems". In: *EPJ Quantum Technology* 6.1 (May 2019). ISSN: 2196-0763. DOI: 10.1140/epjqt/s40507-019-0072-0. URL: http://dx.doi.org/10.1140/epjqt/s40507-019-0072-0.

[4] James F. Annett. *Superconductivity, Superfluids and Condensates*. Oxford Master Series in Condensed Matter Physics. Oxford, UK: Oxford University Press, 2004. ISBN: 9780198507550. DOI: 10.1093/oso/9780198507550.001.0001.

[5] D. M. Lee. "The Discovery of Superfluid Helium-3". In: *JPS Conference Proceedings*. Vol. 38. The Physical Society of Japan, 2020, p. 011001. DOI: 10.7566/JPSCP.38.011001. URL: https://journals.jps.jp/doi/pdf/10.7566/JPSCP.38.011001.

[6] R. Radebaugh and J. D. Siegwarth. "Dilution refrigerator technology". In: *Cryogenics* 11.5 (1971), pp. 368–384. DOI: 10.1016/0011-2275(71)90037-3.

[7] W. L. Johnson. "Cryogenic Multilayer Insulation Theory and Validation". In: *Thermal and Fluids Analysis Workshop (TFAWS 2018)* (NASA Marshall Space Flight Center, Huntsville, AL). NASA Technical Paper. NASA. 2018. URL: https://tfaws.nasa.gov/wp-content/uploads/TFAWS18-CT-05_Paper.pdf.

[8] Alexander T. Holmes et al. "A 17 T horizontal field cryomagnet with rapid sample change designed for beamline use". In: *Review of Scientific Instruments* 83.2 (2012), p. 023904. DOI: 10.1063/1.3682097.

[9] A. T. Ferris. *Cryogenic Strain Gage Techniques for Force Balance Design*. Tech. rep. 19860018146. NASA Technical Paper. NASA, 1986. URL: https://ntrs.nasa.gov/api/citations/19860018146/downloads/19860018146.pdf.

[10] Lake Shore Cryotronics, Inc. *Cernox® Sensors for High-Energy Physics Applications*. Tech. rep. Lake Shore Cryotronics, Inc., 2019.

[11] Michio Watanabe, Masashi Morishita, and Youiti Ootuka. "Magnetoresistance of RuO_2-based resistance thermometers below 0.3 K". In: *Cryogenics* 41.3 (2001), pp. 143–148. DOI: 10.1016/S0011-2275(01)00066-2.

[12] Xiaohe Tang et al. "An optimal piecewise Chebyshev fitting method to calibrate cryogenic temperature sensors". In: *International Conference on Optoelectronic and Microelectronic Technology and Application*. Vol. 11617. SPIE, 2020, p. 116173D. DOI: 10.1117/12.2582395.

[13] Michael A. Johnson and Mohammad H. Moradi. *PID Control*. Springer, 2005.

[14] *Model 370 AC Resistance Bridge / Temperature Controller User's Manual*. Lake Shore Cryotronics, Inc. 2004.

[15] Cryogenic Ltd. *J2942 Cryomagnet System: Manual Drawings*. Cryogenic Ltd. 2010.

A Cryostat Technical Drawing

This technical drawing of the cryostat, provided by Cryogenic Ltd. [15] used in this project is included below.

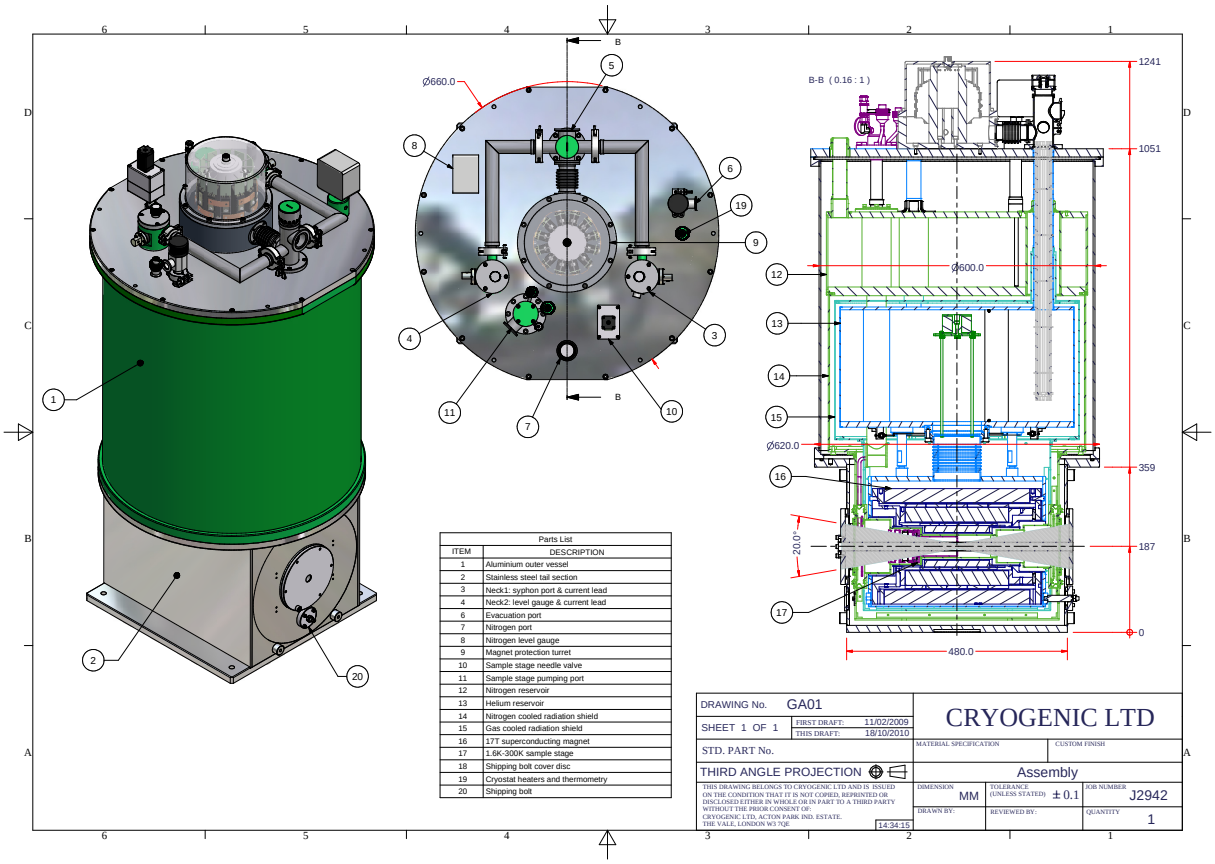

B Calibration Curve for Cernox CX1050

Table 3: Temperature vs Resistance for CX-X97669-MC Thermometer

Temperature (K)	Resistance (Ω)
325	231.110
319	232.388
313.5	233.606
308	234.870
302.5	236.186
297	237.556
291.5	238.982
286	240.468
280.5	242.017
275	243.634
269.5	245.324
264	247.088
258.5	248.934
253.5	250.689
248.5	252.517
243.5	254.425
238.5	256.419
233.5	258.503
228.5	260.682
223.5	262.967
218.5	265.359
213.5	267.867
208.5	270.500
203.5	273.265
198.5	276.175
193.5	279.238
188.5	282.468
183.5	285.871
179	289.101
174.5	292.497
170	296.073
165.5	299.842
161	303.818
156.5	308.019
152	312.467
147.5	317.178
143	322.177
138.5	327.493
134.5	332.510
130.5	337.821
126.5	343.455

Continued on next page

Temperature (K)	Resistance (Ω)
122.5	349.439
118.5	355.812
114.5	362.609
110.5	369.869
106.5	377.650
103	384.931
100.5	390.434
98	396.185
95.5	402.226
93	408.576
90.5	415.250
88	422.292
85.5	429.713
83	437.556
80.5	445.864
78	454.664
75.5	464.016
73.5	471.935
71.5	480.258
69.5	489.032
67.5	498.302
65.5	508.099
63.5	518.476
61.5	529.494
59.4	541.804
57.4	554.320
55.4	567.677
53.6	580.514
51.8	594.165
50	608.735
48.2	624.317
46.4	641.027
44.6	658.993
43	676.150
41.4	694.500
39.7	715.503
38.1	736.844
36.5	759.916
35	783.327
33.5	808.636
32	836.124
30.6	864.037
29.2	894.386
27.9	925.115
26.6	958.563

Continued on next page

Temperature (K)	Resistance (Ω)
25.3	995.221
24.1	1032.342
22.9	1073.045
21.7	1118.005
20.6	1163.613
19.75	1202.231
19.1	1233.939
18.45	1267.758
17.8	1304.037
17.2	1339.904
16.6	1378.298
16	1419.593
15.4	1464.087
14.85	1508.139
14.3	1555.606
13.75	1607.107
13.25	1657.857
12.75	1712.779
12.25	1772.534
11.75	1837.753
11.3	1901.963
10.85	1971.964
10.4	2048.861
9.95	2133.605
9.55	2216.755
9.15	2308.248
8.75	2409.657
8.35	2522.696
7.95	2649.540
7.6	2774.222
7.25	2913.693
6.9	3071.310
6.55	3250.446
6.2	3456.200
5.86	3687.494
5.56	3923.664
5.26	4196.596
4.98	4493.617
4.7	4840.536
4.42	5251.792
4.16	5708.513
3.95	6145.152
3.78	6552.135
3.61	7018.777
3.44	7559.075

Continued on next page

Temperature (K)	Resistance (Ω)
3.28	8151.139
3.13	8796.755
2.98	9551.447
2.83	10 443.820
2.69	11 435.532
2.55	12 620.048
2.41	14 057.366
2.28	15 689.087
2.15	17 693.537
2.03	19 994.616
1.91	22 869.535
1.79	26 549.607
1.68	30 927.927
1.58	36 117.059
1.48	42 950.789
1.4	50 104.468

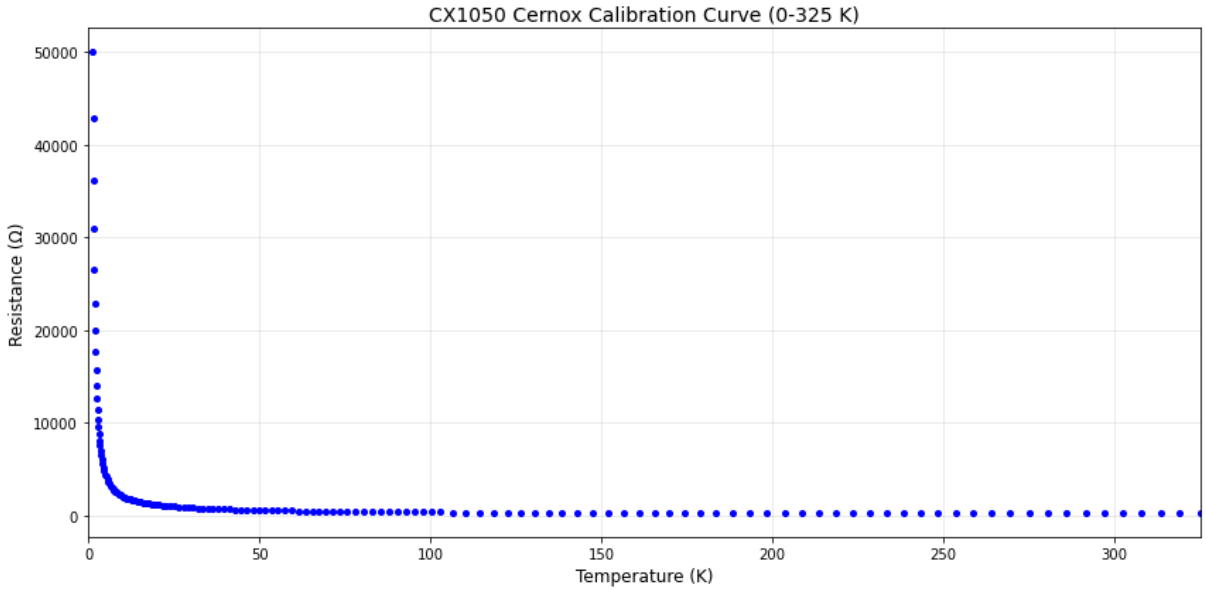

Figure 15: The calibration curve plotted for all the calibration point of the CX1050.

C Sample Cup and Mixing Chamber RuOx Sensor Value Separation

Table 4: Temperature separation between SC and MC RuOx sensors.

Control T (mK)	**Separation (mK)**
250	22.49 ± 4.31
300	35.41 ± 2.95
350	37.74 ± 2.28
400	35.50 ± 6.06
450	42.56 ± 9.02
500	33.63 ± 16.38
550	25.00 ± 16.46
600	27.30 ± 12.19
700	34.19 ± 17.03

D Data or Temperature Control Measurements 250-700 mK

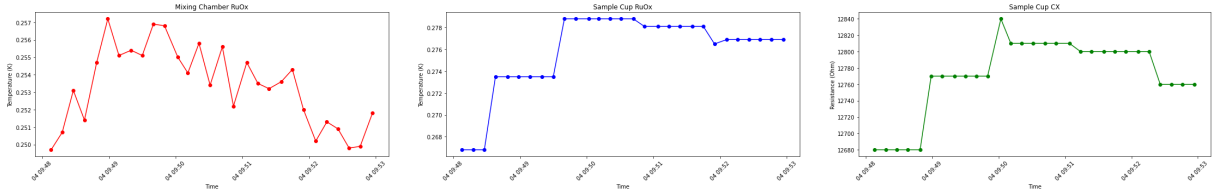

Figure 16: Values at 250 mK. Extracted 09:48-09:53, 04.12.2025.

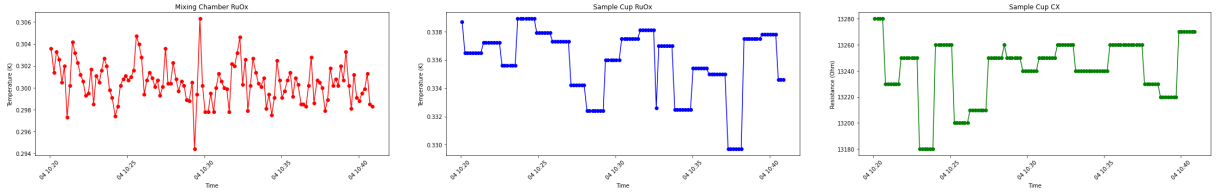

Figure 17: Values at 300 mK. Extracted 10:20-10:40, 04.12.2025.

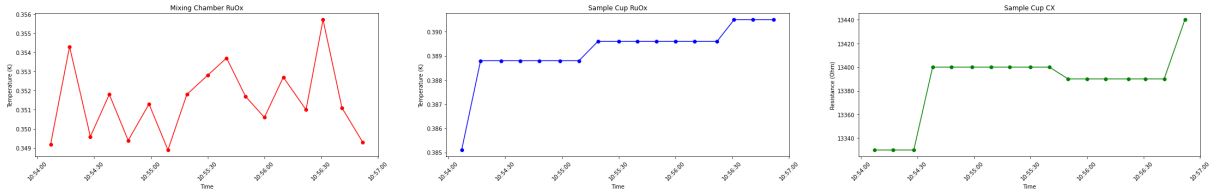

Figure 18: Values at 350 mK. Extracted 10:53-10:57, 04.12.2025.

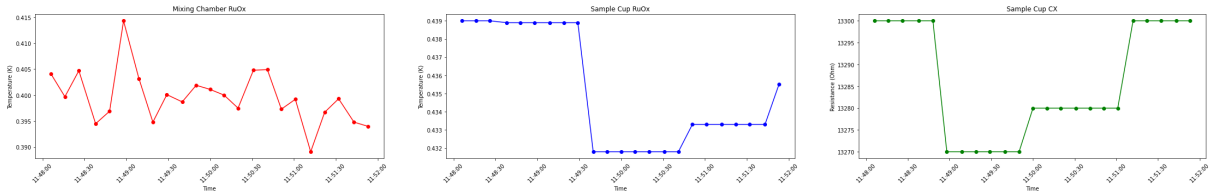

Figure 19: Values at 400 mK. Extracted 11:48-11:52, 04.12.2025.

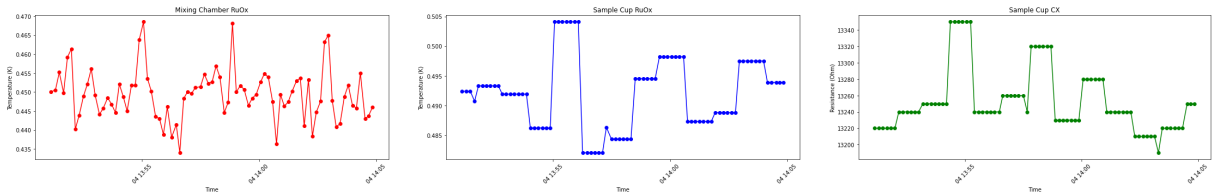

Figure 20: Values at 450 mK. Extracted 13:51-14:05, 04.12.2025.

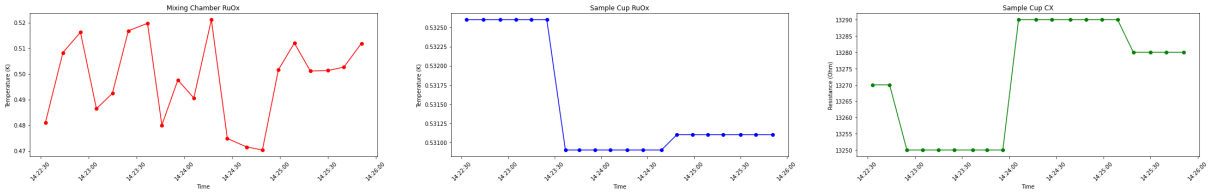

Figure 21: Values at 500 mK. Extracted 14:22-14:26, 04.12.2025.

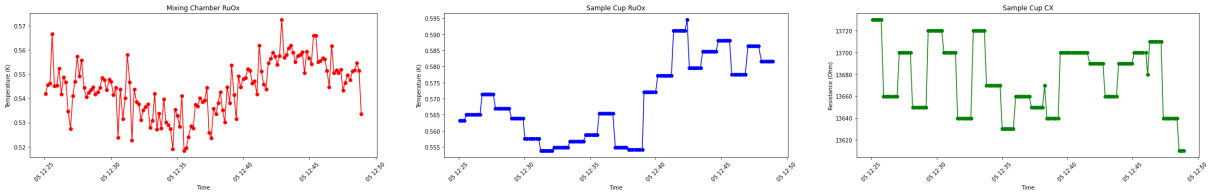

Figure 22: Values at 550 mK. Extracted 12:25-12:49, 05.12.2025.

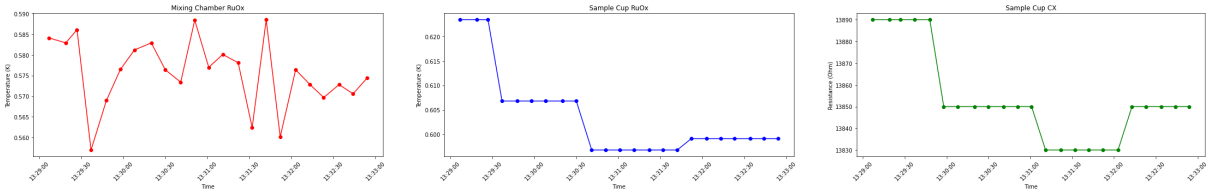

Figure 23: Values at 600 mK. Extracted 13:29-13:33, 05.12.2025.

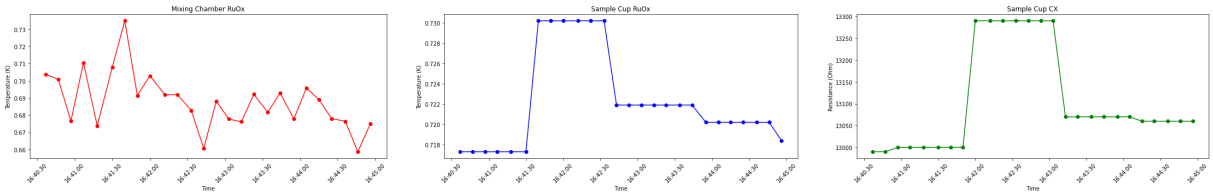

Figure 24: Values at 700 mK. Extracted 16:40-16:45, 05.12.2025.

E Python Code for Chebyshev Polynomial Fitting of CX Calibration Curve

```python
import pandas as pd
import matplotlib.pyplot as plt
import numpy as np
from numpy.polynomial import Chebyshev
from sklearn.model_selection import KFold
from sklearn.metrics import mean_squared_error

filename = r"C:\Users\Omistaja\OneDrive\Documents\Samuel\Lund University\Physics\FYSK04 Bachelor Thesis\Thermometer Calibrations\New calib curves (26.11.25)\CX-1050-SD-HT-1-X97668.340 updated 26.11 +81ohms v3.txt"
df = pd.read_csv(filename, delim_whitespace=True)
df["Resistance"] = 10 ** df["Units"]
df["LogR"] = np.log10(df["Resistance"])

def find_optimal_degree_cv(T, R, deg_range=(3, 15), n_splits=5):
    degrees = range(deg_range[0], deg_range[1] + 1)
    cv_scores = []
    r2_values = []

    kf = KFold(n_splits=n_splits, shuffle=True, random_state=42)

    for deg in degrees:
        try:
            fold_scores = []
            for train_idx, val_idx in kf.split(T):
                T_train, T_val = T[train_idx], T[val_idx]
                R_train, R_val = R[train_idx], R[val_idx]

                cheb_fit = Chebyshev.fit(T_train, R_train, deg)
                R_pred = cheb_fit(T_val)

                mse = mean_squared_error(R_val, R_pred)
                fold_scores.append(mse)

            cv_scores.append(np.mean(fold_scores))

            cheb_fit_full = Chebyshev.fit(T, R, deg)
            R_pred_full = cheb_fit_full(T)
            ss_res = np.sum((R - R_pred_full)**2)
            ss_tot = np.sum((R - np.mean(R))**2)
            r2_values.append(1 - ss_res / ss_tot)

        except Exception as e:
            print(f"Error at degree {deg}: {e}")
            cv_scores.append(np.inf)
            r2_values.append(np.nan)

    best_idx = np.argmin(cv_scores)
    best_deg = list(degrees)[best_idx]
    best_fit = Chebyshev.fit(T, R, best_deg)

    return best_deg, best_fit, list(degrees), cv_scores, r2_values

```

```python
T_min = 1.4
T_max = 4.22
deg_range = (1, 15)
n_splits = 5

T_full = df["Temperature"].values
LogR_full = df["LogR"].values

mask = (T_full >= T_min) & (T_full <= T_max)
T = T_full[mask]
LogR = LogR_full[mask]

deg_opt, cheb_fit, degrees, cv_scores, r2s = find_optimal_degree_cv(
    T, LogR, deg_range, n_splits
)

T_fit = np.linspace(T.min(), T.max(), 500)
LogR_fit = cheb_fit(T_fit)

plt.show()

poly = cheb_fit.convert(kind=np.polynomial.Polynomial)
coeffs = poly.coef
terms = [f"{coeffs[i]:.6g}*T^{i}" if i > 0 else f"{coeffs[i]:.6g}"
         for i in range(len(coeffs))]
equation = " + ".join(terms)
print(f"log10(R) = {equation}")
```